Control of a 5DOF Magnetically Levitated Positioning Stage

Cameron Fulford, Manfredi Maggiore, and Jacob Apkarian

***Abstract*— A high-precision, magnetically levitated, five degree-of-freedom (5DOF) positioning stage is presented. Four independently controlled iron-cored permanent magnet linear synchronous motors are used to translate the stage and rotate it about the two horizontal axes. Six optical encoders with 10 μm resolution, mounted on linear guides, are used to measure displacements and rotations. A partially control-affine model is presented, which is sufficient for the purposes of control. Nonlinear tracking controllers are developed for the 5DOF system using feedback linearization and internal model regulation for step and sinusoidal references.**

I. Introduction

In recent years there has been an increased interest in the development of magnetically levitated (maglev) contactless positioning systems with many degrees-of-freedom (DOF) as an alternative to mechanically-driven high-precision positioning systems. Traditional industrial positioning systems are composed of multiple mechanically-driven stages, some of which actuate large, low-resolution movements, while others deliver small high-resolution motion. Such systems have well-known drawbacks. Friction, stiction, backlash, and hysteresis limit the positioning accuracy. Further, mechanical wear introduces impurities in the form of dust particles into the manufacturing environment. Lastly, mechanical coupling transmits to the microstepper vibrations from the surrounding environment. For those fabrication tasks requiring submicrometer accuracy (e.g., photolithography), such vibrations are unacceptable because they significantly affect the performance of the process, so vibration tables are required.

Maglev positioning stages have the potential to eliminate the three problems mentioned above. Being contactless, their positioning accuracy is only limited by the sensor resolution and the control design. They are not subject to mechanical wear and therefore they do not introduce dust particles in the fabrication process. Finally, they are not mechanically coupled to the surrounding environment and are capable, if appropriately controlled, to reject vibrations.

A landmark contribution to the development of high-precision magnetic levitation actuators was given by Kim and Trumper in [1], see also [2]. They developed a 6DOF positioning system using air-cored permanent magnet linear synchronous motors (PMLSMs) with a horizontal displacement range of 50×50 mm^2, a vertical displacement range of 400 μm, and rotations in the mrad range. The position noise was of the order of 5 nm horizontal and 70 nm vertical. Since then, other significant contributions were made to the development of high-precision contactless positioning systems. Kim and co-workers [3], [4], [5] developed a compact and lightweight device which employs six Lorentz-type linear air-cored actuators to control 6DOF with a displacement range of $300 \times 300 \times 300$ μm^3, a rotation range of $3.5 \times 3.5 \times 3.5$ mrad^3, and a position noise of about 5 nm. Menq and co-workers [6], [7], [8], [9] developed three generations of 6DOF devices. The latest prototype, presented in [9], employs three Lorentz-type two-axis linear actuators to achieve a displacement range of $2 \times 2 \times 2$ mm^3, a rotation range of $70 \times 70 \times 70$ mrad^3, and a position noise of about 4nm horizontal and 20 nm vertical. Other relevant research on this topic is found in [10], [11], [12], [13].

Previous research on maglev systems at the University of Toronto, in collaboration with Quanser, focused on using combinations of iron-cored PMLSMs to control multiple DOFs. In [14], a detailed mathematical model of the forces produced by one PMLSM and a nonlinear control design to regulate air-gap and displacement are presented. The work in [15] presents the implementation of a 2DOF system employing one PMLSM to control longitudinal and vertical displacements, and a 3DOF system employing four PMLSMs to control displacements. In both setups, linear guides are used to constrain the motion to be purely translational. In this paper we go one step forward and show that, with minimal modifications, the four PMLSM device in [15] can be used to control 5DOFs (three displacements and pitch and roll angles) with a range of 100×100 mm^2 horizontal, 13 mm vertical, and rotation range of 6×28 mrad^2. The accuracy is 10 μm for displacements and 20 μrad for rotations. Our device is *not* contactless because it employs linear guides to sense the configuration of the platen, but it is a proof-of-concept giving confidence that our approach can be used to build a next-generation, contactless positioning system.

We present a partially control-affine model, which is an accurate approximation of the detailed mathematical model presented in [16]. Using this partially control-affine model, we develop a nonlinear controller based on feedback linearization and output regulation which accurately tracks step and sinusoidal references.

C. Fulford is with Quanser, 119 Spy Court, Markham, Ontario, Canada L3R 5H6 (e-mail: cameron.fulford@quanser.com). This research was performed while C. Fulford was with the Department of Electrical and Computer Engineering, University of Toronto, Toronto, Ontario, Canada M5S 3G4.

M. Maggiore is with the Department of Electrical and Computer Engineering, University of Toronto, Toronto, Ontario, Canada M5S 3G4 (e-mail: maggiore@control.utoronto.ca).

J. Apkarian is with Quanser, 119 Spy Court, Markham, Ontario, Canada L3R 5H6 (e-mail: jacob.apkarian@quanser.com).

This work was supported by the Natural Sciences and Engineering Research Council of Canada (NSERC), the Canada Foundation for Innovation (CFI), and the Ontario Innovation Trust (OIT).

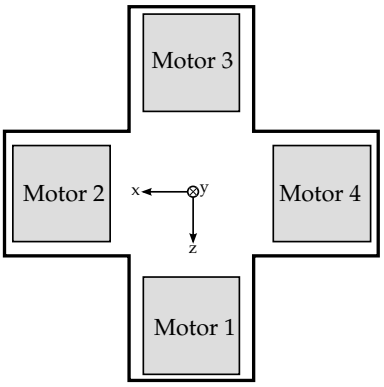

Fig. 1. Top view of the maglev system

II. Hardware and Modeling

Our positioning system consists of a set of four symmetrically placed iron-cored PMLSMs, shown from the top view in Figure 1, where each PMLSM is labeled Motor 1 to Motor 4. Each PMLSM consists of a stator and a mover. The stators, housed in a heavy, stationary frame, are longitudinally laminated and transversally slotted to accommodate a single layer of 3-phase winding. Each mover, consisting of a set of four type N35 permanent magnets, is positioned beneath a corresponding stator and affixed to the aluminum platen. The platen is positioned below the stationary frame and rests on sets of linear guides that allow the platen to move along two horizontal axes, one vertical axis, as well as rotate about the two horizontal axes (pitch and roll). Figure 2 shows the maglev apparatus. Figure 3 illustrates more clearly

Fig. 2. Maglev apparatus viewed from the front

the system of linear guides with directional arrows showing the allowable movement for each set of guides. Note that the top of the vertical Y-axis guides are fixed to the bottom of the platen. As seen in Figure 3, the sets of linear guides are layered such that the Y-axis guides rest on the Z-axis guides, which rest on the X-axis guides. The platen is able to rotate about the X and Z axes since the four vertical guides, although attached to a rigid platen, are independent and can be positioned at different heights, allowing the platen to tilt. While the vertical guides are symmetric with respect to each horizontal axis, they are *not* symmetric with respect to the center of mass of the platen (see Figure 3) because they have a rectangular section. As a result, it is more difficult to rotate about the X-axis than the Z-axis; for this reason, the device can achieve a larger rotation angle about the Z-axis than about the X-axis. Currently, the rigidity of the supporting guides does not allow for rotations about the Y-axis.

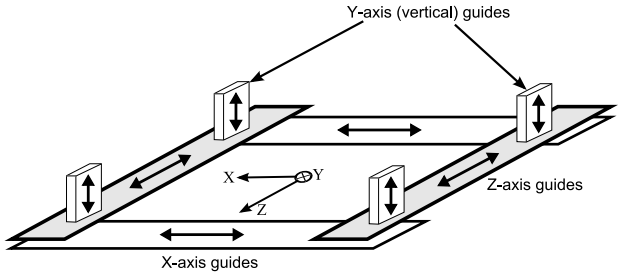

Fig. 3. Linear guides with arrows indicating the direction of movement of the guides

The linear guides do not provide any force to the platen other than friction and are necessary at this stage to maintain proper alignment of the platen and, most importantly, facilitate the placement of sensors used to measure displacements of the platen. The 3DOF apparatus in [15] uses three optical encoders mounted on the linear guides to measure X-axis, Z-axis, and Y-axis displacement. For the 5DOF system there are a total of six optical encoders mounted on the guides: two sensors measuring horizontal displacements along the X-axis and Z-axis, and four sensors mounted on the four vertical guides that are used to measure vertical displacement and also rotations about the X-axis and Z-axis. The linear guides also allow us to insert stoppers to constrain the motion of the platen, which is useful for parameter estimation purposes. The system has a horizontal displacement range of ± 50mm along the X-axis and Z-axis, a vertical range of approximately 13mm, and rotations about the X-axis and Z-axis of approximately ± 3mrad and ± 14mrad, respectively. Aside from the limitations on the rotations imposed by the rigidity of the linear guides, the maximum rotation angles are also limited at small and large air-gaps where we risk hitting the stoppers. The 5DOF apparatus has a translational resolution of 10μm and a rotational resolution of approximately 20μrad.

The 5DOF system uses four custom-built power supplies developed by Quanser, each capable of delivering approximately 5 A continuous and 10 A peak current. Each power supply is connected to a single PMLSM so that the four PMLSMs can be independently controlled. Conceptually, we want to control the displacement of the movers/platen in several directions by applying current to the stators. The reader is referred to [14], [15] for the details of the iron-cored PMLSM operation and modeling.

For a single stator/mover pair, the horizontal force (F_H) and vertical force (F_V) exerted on the mover by the stator are given by

$$F_H(g, i_q) = -K_h L_h(g) i_q \tag{1}$$

$$F_V(g, i_q, i_d) = \begin{array}{l} -K_{v1} L_{v1}(g) + K_{v2} L_{v2}(g) i_d - \\ K_{v3} L_{v3}(g)(i_d^2 + i_q^2), \end{array} \tag{2}$$

where

$$
\begin{aligned}
K_{v1} &= \tfrac{L_A p_m \tau}{4\mu_0},\\
K_{v2} &= \tfrac{3\sqrt{2} L_A p_m W k_{w1}}{p^2},\\
K_{v3} &= \tfrac{18 L_A p_m W^2 k_{w1}^2 \mu_0}{\tau p^2},\\
L_{v1}(g) &= \tilde{\lambda}(g) B_{pmy1}^2(g),\\
L_{v2}(g) &= \tfrac{\tilde{\lambda}(g) B_{pmy1}(g) \coth(\frac{\pi}{\tau}(h_m+g))}{K_c(g)},\\
L_{v3}(g) &= \tfrac{\tilde{\lambda}(g) \coth^2(\frac{\pi}{\tau}(h_m+g))}{K_c^2(g)},
\end{aligned}
\tag{3}
$$

and

$$
\begin{aligned}
K_h &= \frac{12\sqrt{2} W k_{w1} p_m L_A \sigma_m \mu_0 \sinh(\frac{\pi}{\tau} h_m) \sin(\frac{\pi \tau_p}{2\tau})}{\pi p},\\
L_h(g) &= \frac{\tilde{\lambda}(g)}{K_c(g) \sinh(\frac{\pi}{\tau}(h_m+g))},\\
K_c(g) &= \frac{t_1}{t_1 - g\gamma_1(g)},\\
\gamma_1(g) &= \frac{4}{\pi}\left[\frac{b_0}{2g}\arctan\left(\frac{b_0}{2g}\right) - \ln\sqrt{1+\left(\frac{b_0}{2g}\right)^2}\right],\\
\tilde{\lambda}(g) &= 1 - \frac{b_0^2}{4t_1(g + \frac{b_0}{2} + \frac{h_m}{\mu_{rec}})}.
\end{aligned}
\tag{4}
$$

In the force expressions (1), (2), i_d and i_q represent the direct and quadrature currents applied to the three-phase winding of the stator, while g is the vertical air-gap, i.e., the distance between the mover and stator. The physical parameters in the above equations are given in [16]. Note that in the equation for the vertical force (F_V) is not affine in the controls i_d and i_q.

In order to model the motion of the platen with the configuration shown in Figure 1, we assume that its center of mass (CM) coincides with its geometric center, and define the state vector $(x_1, \ldots, x_{10})$ as in Table I. Note that the

TABLE I

STATE VARIABLES AND THEIR PHYSICAL MEANING FOR THE 5DOF MAGLEV SYSTEM

State variable	Units	Description
x_1	m	Vertical displacement of CM
x_2	m/s	Vertical velocity of CM
x_3	m	X-axis displacement of CM
x_4	m/s	X-axis velocity of CM
x_5	m	Z-axis displacement of CM
x_6	m/s	Z-axis velocity of CM
x_7	rad	Rot. angle about the X-axis (ϕ)
x_8	rad/s	Ang. vel. about the X-axis
x_9	rad	Rot. angle about the Z-axis (θ)
x_{10}	rad/s	Ang. vel. about the Z-axis

state x_1, the vertical displacement of the center of mass of the platen, corresponds to the average air-gap of the four PMLSMs, which we denote $g_1, \ldots, g_4$. Therefore, letting r denote the distance from the center of the platen to the center of the movers,

$$
\begin{aligned}
g_1 &= x_1 - r\sin x_7\\
g_2 &= x_1 + r\sin x_9\\
g_3 &= x_1 + r\sin x_7\\
g_4 &= x_1 - r\sin x_9.
\end{aligned}
\tag{5}
$$

We combine the horizontal forces as follows. We impose that the quadrature currents for Motors 2 and 4 (lying along the X-axis) be equal, and we denote u_x the resulting quadrature current. Similarly, we impose that the quadrature currents for Motors 1 and 4 (lying along the Z-axis) be equal to a current u_z. We then let the direct currents i_d be redefined as inputs $u_{y1}, \ldots, u_{y4}$ for Motors 1 to 4, respectively. Thus, the forces applied to the 5DOF system are as illustrated in Figure 4.

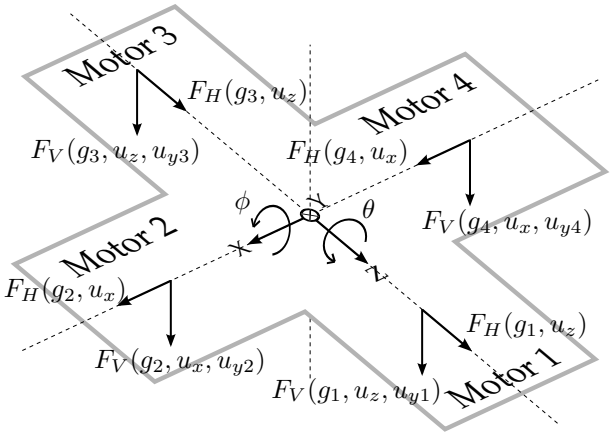

Fig. 4. PMLSM forces for the 5-DOF system

We define control inputs $v = (v_y, v_\phi, v_\theta)$ by the input transformation, $(u_{y1}, u_{y2}, u_{y3}, u_{y4}) \mapsto (v_y, v_\phi, v_\theta)$ defined as:

$$
\begin{aligned}
v_y &= u_{y2} + u_{y4}\\
v_y &= u_{y1} + u_{y3}\\
v_\phi &= u_{y1} - u_{y3}\\
v_\theta &= u_{y4} - u_{y2},
\end{aligned}
\tag{6}
$$

where now v_y controls the vertical translation, v_ϕ controls the X-axis rotation, and v_θ controls the Z-axis rotation. Thus using the controls $u = (u_x, u_z)$ and v we have a total of five inputs to control five DOFs. The (ϕ, θ) rotations are controlled by exerting different normal forces at opposite ends of the apparatus using Motor pairs 1/3 and 2/4, thus applying a torque about the horizontal axes. Let I_x and I_z denote the moments of inertia about the X-axis and Z-axis (by symmetry, $I_x = I_z$), and define M_y, M_x, and M_z as the mass on the Y-axis, X-axis, and Z-axis guides, respectively. The partially control-affine 5DOF model reads as:

$$\dot{x} = \begin{bmatrix} x_2 \\ a_1 \\ x_4 \\ h_x(x_1, x_9)u_x \\ x_6 \\ h_z(x_1, x_7)u_z \\ x_8 \\ b_1 \\ x_{10} \\ c_1 \end{bmatrix} + \begin{bmatrix} 0 & 0 & 0 \\ a_3 & a_2 & a_4 \\ 0 & 0 & 0 \\ 0 & 0 & 0 \\ 0 & 0 & 0 \\ 0 & 0 & 0 \\ 0 & 0 & 0 \\ b_3 & b_2 & 0 \\ 0 & 0 & 0 \\ c_3 & 0 & c_2 \end{bmatrix} v, \qquad (7)$$
$$y = \begin{bmatrix} x_1 & x_3 & x_5 & x_7 & x_9 \end{bmatrix}^\top,$$

where y is the output of the system and the terms in the above dynamics are given in [16]. Note that the model (7) is affine in the control v.

III. Nonlinear Controller Design

In this section, we design a controller to track steps and sinusoidal reference signals with a given frequency ω_0. Consider the model (7) and the following feedback linearizing transformation:

$$\begin{bmatrix} v_y \\ v_\phi \\ v_\theta \end{bmatrix} = M^{-1} \begin{bmatrix} w_1 - a_1 \\ w_4 - b_1 \\ w_5 - c_1 \end{bmatrix} \quad \begin{bmatrix} u_x \\ u_z \end{bmatrix} = \begin{bmatrix} \dfrac{w_2}{h_x(x_1, x_9)} \\ \dfrac{w_3}{h_z(x_1, x_7)} \end{bmatrix}, \qquad (8)$$

where

$$M = \begin{bmatrix} a_3 & a_2 & a_4 \\ b_3 & b_2 & 0 \\ c_3 & 0 & c_2 \end{bmatrix}, \qquad (9)$$

and $w_1, \ldots, w_5$ are new control inputs. The state-dependent matrix M can be numerically shown to be invertible in the range of operation of the system and $h_x(x_1, x_9)$ and $h_z(x_1, x_7)$ are non-zero within the operating range. The closed-loop (CL) system reads as:

$$\begin{aligned} \dot{x}_1 &= x_2 \\ \dot{x}_2 &= w_1 \\ \dot{x}_3 &= x_4 \\ \dot{x}_4 &= w_2 \\ \dot{x}_5 &= x_6 \\ \dot{x}_6 &= w_3 \\ \dot{x}_7 &= x_8 \\ \dot{x}_8 &= w_4 \\ \dot{x}_9 &= x_{10} \\ \dot{x}_{10} &= w_5 \\ y &= \begin{bmatrix} x_1 & x_3 & x_5 & x_7 & x_9 \end{bmatrix}^T \end{aligned} \qquad (10)$$

Now we have a linear system composed of five double integrators with input $(w_1, w_2, w_3, w_4, w_5)$ and output y.

A. Tracking Controller Design

We now apply the output regulation theory of [17], [18], [19] to (10). The control objective is to stabilize set-point references, track sinusoidal references with fixed frequency ω_0, or a combination of the two. Since (10) comprises five decoupled linear systems, each with two poles at the origin, it would be sufficient, in principle, to use internal models with poles at $\pm i\omega_0$. In order to provide robustness against constant input disturbances, we also include a pole at the origin. In conclusion, the output regulator incorporates five structurally identical internal models with poles at $\pm i\omega_0$ and 0

$$\begin{aligned} \dot{\xi}_y &= \Phi\xi_y + Ne_y, \quad w_1 = \Gamma\xi_y \\ \dot{\xi}_x &= \Phi\xi_x + Ne_x, \quad w_2 = \Gamma\xi_x \\ \dot{\xi}_z &= \Phi\xi_z + Ne_z, \quad w_3 = \Gamma\xi_z \\ \dot{\xi}_\phi &= \Phi\xi_\phi + Ne_\phi, \quad w_4 = \Gamma\xi_\phi \\ \dot{\xi}_\theta &= \Phi\xi_\theta + Ne_\theta, \quad w_5 = \Gamma\xi_\theta, \end{aligned} \qquad (11)$$

where

$$\Phi = \begin{bmatrix} 0 & 1 & 0 \\ 0 & 0 & 1 \\ 0 & -\omega_0^2 & 0 \end{bmatrix}, \quad N = \begin{bmatrix} 0 \\ 0 \\ 1 \end{bmatrix}, \quad \Gamma = \begin{bmatrix} 1 & 0 & 0 \end{bmatrix}, \qquad (12)$$

and $e_y = x_1 - x_1^{\text{ref}}$, $e_x = x_3 - x_3^{\text{ref}}$, $e_z = x_5 - x_5^{\text{ref}}$, $e_\phi = x_7 - x_7^{\text{ref}}$, $e_\theta = x_9 - x_9^{\text{ref}}$ denote the tracking errors. The regulator design is completed by letting

$$\begin{aligned} w_1 &= K_y \begin{bmatrix} e_y \\ \dot{e}_y \\ \xi_y \end{bmatrix} + \Gamma\xi_y, \quad w_2 = K_x \begin{bmatrix} e_x \\ \dot{e}_x \\ \xi_x \end{bmatrix} + \Gamma\xi_x, \\ w_3 &= K_z \begin{bmatrix} e_z \\ \dot{e}_z \\ \xi_z \end{bmatrix} + \Gamma\xi_z, \quad w_4 = K_\phi \begin{bmatrix} e_\phi \\ \dot{e}_\phi \\ \xi_\phi \end{bmatrix} + \Gamma\xi_\phi, \\ w_5 &= K_\theta \begin{bmatrix} e_\theta \\ \dot{e}_\theta \\ \xi_\theta \end{bmatrix} + \Gamma\xi_\theta. \end{aligned} \qquad (13)$$

The state feedback controller gains $K_y, K_x, K_z, K_\phi, K_\theta$ are chosen to stabilize the system (10) augmented with the regulator system (11) with the inputs $w_1, \ldots, w_5$ are chosen as in (13) and the references $x_1^{ref}, \ldots, x_9^{ref}$ set to zero.

We also include saturations and antiwindup compensators for the horizontal X-axis and Z-axis regulators since large step references for the horizontal translations result in large translational accelerations and demand larger sustained currents, which pushes the limits of the current amplifiers. Letting $\text{sat}_7(u)$ denote the saturation function with saturation limits at ± 7, the antiwindup compensators for the X and Z-axes internal models are defined as

$$\begin{aligned} \dot{\xi}_x &= \Phi\xi_x + Ne_x + E_{cx}\big(\text{sat}_7(u_x) - u_x\big), \quad w_2 = \Gamma\xi_x \\ \dot{\xi}_z &= \Phi\xi_z + Ne_z + E_{cz}\big(\text{sat}_7(u_z) - u_z\big), \quad w_3 = \Gamma\xi_z, \end{aligned} \qquad (14)$$

where E_{cx} and E_{cz} are antiwindup compensator gains that are manually tuned to give the desired antiwindup performance (stability and minimal overshoot) for aggressive internal model regulator design (fast transients, minimal steady-state error). The final controller is given by (8), (11), (13), and (14). A block diagram of the closed-loop system is shown in Figure 5.

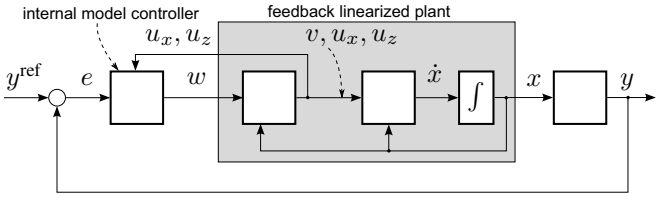

Fig. 5. Block diagram of the 5DOF system with tracking controller

IV. Experimental Results

As mentioned in Section II, the range of rotation about the X-axis is smaller than that about the Z-axis due to the asymmetry of the vertical guides. Therefore, we will implement a regulator for the X-axis rotation to regulate that angle to zero and only show experimental results for set-point stabilization and sinusoidal tracking for the Z-axis rotation, which has a much larger range of operation. We stress that experimental results for the Z-axis rotation give similar results to those associated with the X-axis rotation, the main differences being a degradation in performance and reduced range of rotation. We also stress that once the linear guides are removed from the apparatus, the adverse effect of linear guides on rotations will disappear and there should be no difference between X-axis and Z-axis rotations.

A. Set-Point Stabilization

We begin by performing set-point stabilization for the 3DOF translational subsystem (states $x_1, \ldots, x_6$). The rotation controls are disabled ($v_\phi = v_\theta = 0$) to ensure that all four motors produce equal normal forces to lift the platen evenly. The values chosen for $K_y, K_x, K_z, K_\phi, K_\theta$ are generated using LQR design with manual tuning of the weight matrices. The resulting closed-loop poles of the $(e_y, \dot{e}_y, \xi_y)$ subsystem are $[-173.2, -2.61 \pm i\,5.48, -2.16 \pm i\,1.77]$ and the closed loop poles of the $(e_x, \dot{e}_x, \xi_x)$ and $(e_z, \dot{e}_z, \xi_z)$ subsystems are $[-38.73, -3.2 \pm i\,5.89, -2.69 \pm i\,2.23]$. Saturations and antiwindup compensators are included and the manually tuned antiwindup compensator gains are $E_{cx} = E_{cz} = 7 \times 10^{-5}[1 \quad 1 \quad 1]^\top$. The output x_1 and absolute position error $|x_1 - x_1^{ref}|$ are shown in Figure 6.

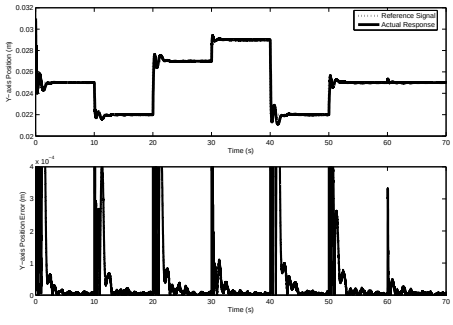

Fig. 6. Y-axis response and error for 3DOF set-point stabilization

It is noted that the controller gains can be tuned to reduce the settling time at the expense of increased overshoot. To reduce the overshoot for step references we can choose to accept a longer settling time or reduce the step size. This trade-off between overshoot and settling time was also observed in [15].

Next, we control one rotation, the rotation about the Z-axis. We restrict the horizontal motion of the platen in hardware so that the platen can only move along the vertical Y-axis and rotate. Since we cannot fix the center of mass of the platen without also restricting rotations, we use the Y-axis regulator to maintain a constant air-gap of 25mm. Throughout these tests there is negligible deviation from the desired air-gap. After tuning the rotation regulator gains using LQR, the closed-loop poles of the $(e_\theta, \dot{e}_\theta, \xi_\theta)$ subsystem are $[-200, -2.81 \pm i\,5.58, -2.19 \pm i\,1.82]$. A series of step commands are issued to the Z-axis rotation (angle θ), and the results are shown in Figure 7.

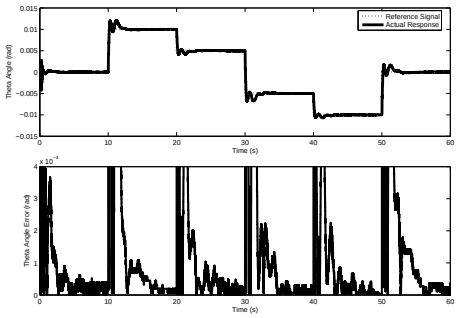

Fig. 7. Z-axis rotation response and error for 1DOF set-point stabilization

The set-point stabilization results for the three translations and one rotation show overshoots less than 30%, settling times under 3s for translations and under 5s for rotation, and steady-state errors reaching encoder resolution in under 10s. Similar set-point stabilization experiments for the X-axis rotation (results omitted) exhibit a degraded performance and a smaller range of operation compared to the Z-axis rotation, which is due to the effects of the vertical guides opposing rotations.

B. Sinusoidal Tracking

We apply sinusoidal reference signals with a frequency $\omega_0 = 1.5\pi$rad/s. Set $\omega_0 = 1.5\pi$ in the internal models (12) and (11). Using the same controller gains developed for 4DOF set-point stabilization, the following reference commands are used to actuate the Y/X/Z-axis translations and the Z-axis rotation:

$$\begin{aligned} x_1^{ref}(t) &= 0.005\sin(1.5\pi t - \pi/2) + 0.025 \\ x_3^{ref}(t) &= 0.03\sin(1.5\pi t - \pi/2) \\ x_5^{ref}(t) &= 0.03\sin(1.5\pi t) \\ x_7^{ref}(t) &= 0 \\ x_9^{ref}(t) &= 0.01\sin(1.5\pi t). \end{aligned} \tag{15}$$

Figure 8 shows the response of the Y-axis position and tracking error. Figure 9 shows the response of the Z-axis rotation angle and tracking error. The average position and rotation tracking errors measured over 60 seconds are

$$
\begin{aligned}
x_1^{err} &= 47.03\mu\text{m} \\
x_3^{err} &= 77.98\mu\text{m} \\
x_5^{err} &= 76.85\mu\text{m} \\
x_9^{err} &= 123.9\mu\text{rad}.
\end{aligned} \tag{16}
$$

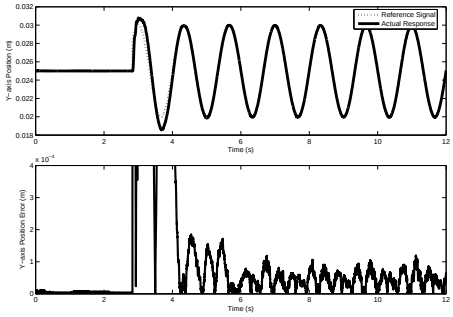

Fig. 8. Y-axis response and error for 4DOF sinusoidal tracking

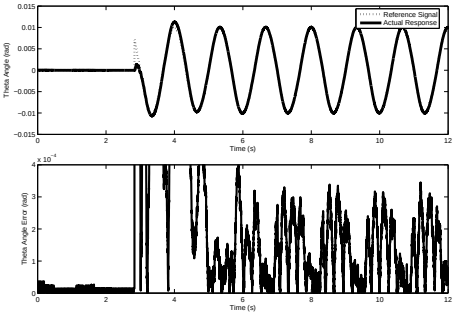

Fig. 9. Z-axis rotation response and error for 4DOF sinusoidal tracking

V. Conclusions

In this paper, the problem of controlling rotations (pitch and roll) of a magnetically levitated positioning system using iron-cored PMLSMs has been addressed. The internal model regulator controller design successfully stabilizes set-point references and tracks sinusoidal references of a given frequency for XYZ translations and rotations about the X-axis and Z-axis. The results indicate that it is possible to remove the linear guide system supporting the platen and achieve fully contactless levitation with 5 degrees-of-freedom. It is noted that we have not addressed the issue of controlling the yaw of the platen. Controlling the yaw (or at least constraining this rotation) is necessary in order to ensure the current apparatus can operate without supporting linear guides. Control of the yaw rotation as well as the implementation of contactless sensing equipment for output measurement will be the subject of future research.

VI. Acknowledgement

We wish to thank Tyler Ackland at Quanser for his help with upgrading the magnetic levitation experiment.

References

[1] W. Kim and D. Trumper, "High-precision levitation stage for photolithography," *Precision Engineering*, vol. 22, pp. 66–77, 1998.

[2] W. Kim, D. L. Trumper, and J. H. Lang, "Modeling and vector control of planar magnetic levitator," *IEEE Transactions on Industry Applications*, vol. 34, no. 6, pp. 1254–1262, November/December 1998.

[3] S. Verma, W. jong Kim, and H. Shakir, "Multi-axis maglev nanopositioner for precision manufacturing and manipulation applications," *IEEE Transactions on Industry Applications*, vol. 41, no. 5, pp. 1159–1167, 2005.

[4] S. Verma, W. jong Kim, and J. Gu, "Six-axis nanopositioning device with precision magnetic levitation technology," *IEEE/ASME Transactions on Mechatronics*, vol. 9, no. 2, pp. 384–391, 2004.

[5] J. Gu, W. jong Kim, and S. Verma, "Nanoscale motion control with a compact minimum-actuator magnetic levitator," *Journal of Dynamic Systems, Measurement, and Control*, vol. 127, pp. 433–442, 2005.

[6] X. Shan, S.-K. Kuo, J. Zhang, and C.-H. Menq, "Ultra precision motion control of a multiple degree of freedom magnetic suspension stage," *IEEE/ASME Transactions on Mechatronics*, vol. 7, no. 1, pp. 67–78, March 2002.

[7] S.-K. Kuo, X. Shan, and C.-H. Menq, "Large travel ultra precision x-y-θ motion control of a magnetic suspension stage," *IEEE/ASME Transactions on Mechatronics*, vol. 8, no. 3, pp. 334–341, 2003.

[8] S.-K. Kuo and C.-H. Menq, "Modeling and control of a six-axis precision motion control stage," *IEEE/ASME Transactions on Mechatronics*, vol. 10, no. 1, pp. 50–59, 2005.

[9] Z. Zhang and C.-H. Menq, "Six-axis magnetic levitation and motion control," *IEEE Transactions on Robotics*, vol. 23, no. 2, pp. 196–205, 2007.

[10] F. Auer and H. F. van Beek, "Practical application of a magnetic bearing and linear propulsion unit for six degree of freedom positioning," in *Fourth International Symposium on Magnetic Bearings*, Zurich,Switzerland, August 1994, pp. 183–188.

[11] A. Molenaar, F. Auer, and H. F. van Beek, "Application of magnetic bearing for contactless ultra high precision positioning," in *Fifth International Symposium on Magnetic Bearings*, Kanazawa, Japan, August 1996, pp. 441–445.

[12] A. Molenaar, E. H. Zaaijer, and H. F. van Beek, "A novel low dissipation long stroke planar magnetic suspension and propulsion stage," in *Sixth International Symposium on Magnetic Bearings*, Boston, MA, USA, August 1998, pp. 650–659.

[13] K. S. Jung and Y. S. Baek, "Study on a novel contact-free planar system using direct drive DC coils and permanent magnets," *IEEE/ASME Transactions on Mechatronics*, vol. 2, pp. 25–43, 2002.

[14] M. Maggiore and R. Becerril, "Modeling and control design for a magnetic levitation system," *International Journal of Control*, vol. 77, no. 10, pp. 964–977, 2004.

[15] R. B. Owen and M. Maggiore, "A high-precision, magnetically levitated positioning stage: Toward contactless actuation for industrial manufacturing," *Control Systems Magazine*, vol. 26, no. 3, pp. 82–95, 2006.

[16] C. Fulford, "Control of a high-precision positioning system using magnetic levitation," Master's thesis, Dept. of Electrical Engineering, University of Toronto, 10 Kings's College Road, Toronto, Ontario, M5S 3G4, 2007.

[17] E. J. Davison, "The robust control of a servomechanism problem for linear time-invariant multivariable systems," *IEEE Transactions on Automatic Control*, vol. 21, pp. 25–34, 1976.

[18] B. A. Francis, "The linear multivariable regulator problem," *SIAM Journal on Control and Optimation*, vol. 14, pp. 486–505, 1977.

[19] B. A. Francis and W. M. Wonham, "The internal model principle of control theory," *Automatica*, vol. 12, pp. 457–465, 1976.